

Review

Bioimaging Applications of Carbon Nanodots: A Review

Athanasia Kasouni ¹, Theodoros Chatzimitakos ^{2,*}  and Constantine Stalikas ²

¹ Laboratory of Biophysical Chemistry, Department of Biological Applications and Technologies, University of Ioannina, 45110 Ioannina, Greece; athanasia_kasouni@yahoo.gr

² Laboratory of Analytical Chemistry, Department of Chemistry, University of Ioannina, 45110 Ioannina, Greece; cstalika@uoi.gr

* Correspondence: chatzimitakos@outlook.com; Tel.: +30-265-100-8725

Received: 31 March 2019; Accepted: 16 April 2019; Published: 22 April 2019



Abstract: Carbon nanodots (CNDs) is the newest member of carbon-based nanomaterials and one of the most promising for the development of new, advanced applications. Owing to their unique and unparalleled physicochemical and photoluminescent properties, they are considered to be a rising star among nanomaterials. During the last decade, many applications have been developed based on CNDs. Among others, they have been used as bioimaging agents to label cells and tissues. In this review, we will discuss the advancements in the applications of CNDs in the field of imaging, in all types of organisms (i.e., prokaryotes, eukaryotes, and animals). Selective imaging of one type of cells over another, imaging of (bio)molecules inside cells and tumor-targeting imaging are some of the studies that will be discussed hereafter. We hope that this review will assist researchers with obtaining a holistic view of the developed applications and hit on new ideas so that more advanced applications can be developed in the near future.

Keywords: carbon nanodots; imaging; labeling; biosensing; bacteria; fungi; eukaryotic cells; animals; mice; zebrafish

1. Introduction

The research interest surrounding nanomaterials continues to grow unabated as more and more scientists are involved in relevant research fields, aiming to exploit the expanding range of novel applications of nanomaterials [1]. Advancements in the development of innovative nanomaterials have led to the synthesis of carbon quantum dots or carbon nanodots (CNDs). CNDs belong to a newly discovered, up-and-coming class of quasi-spherical carbon nanomaterials, whose size is lower than 10 nm [2]. They combine the unique optical properties of the “traditional” semiconductor quantum dots with the prominent electrical properties which derive from the sp² carbon. These properties result in a significant differentiation from other classes of nanomaterials [3]. Additionally, the substantive amount of oxygenic moieties integrated on the surface of CNDs endows them with splendid dispersibility in aqueous solutions and makes feasible their functionalization with other compounds. Moreover, the structural characteristics of CNDs endow them with several key merits, such as tunable photoluminescence (PL) accompanied by resistance to photobleaching, moderate quantum yield (QY), chemical inertness, low cytotoxicity towards eukaryotic cells, etc. Owing to these outstanding features, CNDs are utilized in an increasing number of applications nowadays [4–6].

Since the serendipitous discovery of carbon dots over a decade ago, research into their formation and application has grown exponentially and an increased interest in introducing them into health-, environmental-, and technological-related applications has emerged [7]. Moreover, it was not until recently that CNDs were used as antibacterial agents, fluorescent agents, drug carriers, and probes for

the *in vitro* and *in vivo* detection of specific molecules, and they have even been proposed for human cancer theranostic and phototherapy applications [8–12]. Not surprisingly, therefore, CNDs can be considered to be the next generation platform for biomedical applications.

In this context, numerous studies have been published regarding imaging applications and their number keeps increasing at a high rate. The imaging potential of the CNDs has been examined in many different (micro)organisms (from prokaryotes to mammals). However, owing to the “myriads” of studies around the topic, it is difficult to have a holistic view of the scientific advancements in the field. In this review, we focus on the imaging applications of CNDs to all types of organisms (i.e., prokaryotes, eukaryotes, and animals), and we highlight specific studies that contributed substantially or deserve considerable attention to obtain a better understanding of the topic. Moreover, exceptional and “unconventional” imaging applications are discussed, so as the horizons of researches to be expanded with the aim of developing more advanced applications.

2. Synthesis of CNDs

The physicochemical properties of the CNDs, and thus, their potential for various applications, are dependent on the precursor materials employed and the synthesis method. The synthesis of the CNDs can be divided into two main categories: the bottom-up and the top-down approaches. Within the bottom-up approach lie the procedures in which simple materials are used to “grow” CNDs. In contrast, breaking down macroscopic materials (such as food products and plants) to produce CNDs, is the principle of top-down approach [3,13]. Many different materials have been used to develop CNDs, including apple seeds [14], *Citrus sinensis* or *Citrus limon* peels [15], human fingernails [16,17], cotton [18], citrulline [19], coriander leaves [20], carrot juice [21], citric acid and tris(hydroxymethyl) methylaminomethane [22], polyethyleneimine, nitric acid [23], and many others. Additionally, many different procedures can be employed to produce CNDs, with the most commonly employed method being the solvothermal carbonization, pyrolysis, and microwave treatment [7,24–27]. As the number of precursor materials is enormous and the number of possible combinations is even higher, it is easily conceivable that a wide variety of CNDs can be prepared [28,29].

3. Imaging Applications for Bacteria and Fungi

Up to now, many different protocols have been developed to stain bacteria species to address the need for fast and accurate bacteria detection. In this context, CNDs have been developed for imaging of various bacteria species. Das et al. developed CNDs by heating gram shells at 315 °C for 3 h. The synthesized CNDs had tunable PL, which enabled the multicolor imaging of *Escherichia coli* (*E. coli*) cells after incubation with the CNDs for 3 h [30]. In this case, the imaging was based on the properties of the CNDs to attach to the bacterial cell surface. In another study, Pal et al. prepared N-doped CNDs by treating hydrothermally a mixture of curcumin and polyethyleneimine [31]. The synthesized CNDs were used for the multicolor imaging of *E. coli* and *Staphylococcus aureus* (*S. aureus*), after incubation with the CNDs for 3 h. Despite the differences in the cell membrane of the two-bacterial species, the CNDs could be used for both of them, making the material potent imaging agent. Moreover, the examined CNDs did not exhibit bactericidal activity against the two bacterial species, allowing the observation of live bacterial cells. In a similar concept, Baig and Chen synthesized CNDs from egg whites [32]. These CNDs were also suitable for multicolor *E. coli* and *S. aureus* imaging, as in the previous case (Figure 1). However, their CNDs had a much greater QY (45%) and labeled bacteria after only 10 min of incubation. This property made feasible faster labeling of bacteria with a lower amount of CNDs (bacteria were labeled using 1 µL of 0.1 mg mL⁻¹ CNDs solution, in contrast to 100 µL of CNDs solution with the same concentration in the previous case). In another study, N,S-codoped CNDs were prepared by microwave heating of a mixture of tris-acetate-ethylenediamine buffer and thiourea [33]. The QY of the resulting CNDs was high (57%), making it possible for them to be used for the efficient multicolor labeling of bacteria. In this case, the authors examined four bacteria species: *E. coli*, *S. aureus*, *Pseudomonas aeruginosa* (*P. aeruginosa*), and *Klebsiella pneumoniae* (*K. pneumoniae*). The first

three species can efficiently be labeled, owing to endocytosis of the CNDs. The *K. pneumoniae* cells were not fluorescent after incubation under the same conditions. This was attributed to the catabolic pathways that *K. pneumoniae* expresses for various aromatic compounds, which can “decimate” the CNDs. This finding is important because it shows that CNDs are not suitable for a number of bacteria species, owing to the high diversity that is noted among them. Wang et al. used a mixture of sodium citrate, urea, and thiourea to prepare excitation independent CNDs with a QY of 37% [34]. These CNDs emitted blue fluorescence and, as a consequence, *Xanthomonas axonopodis* cells incubated for 3 h with the CNDs were blue fluorescent under UV light. In this case, bacteria were also stained alive and no disruption of their morphology was observed.

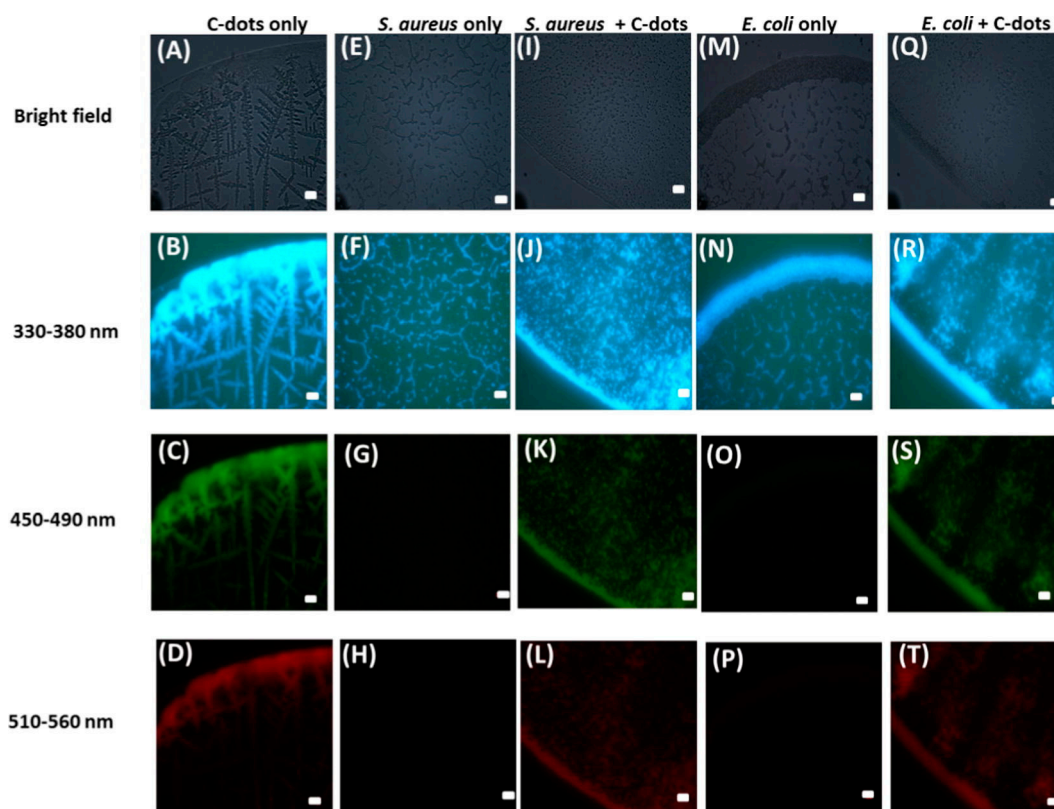


Figure 1. Fluorescence microscopic images (A–D) of C-dots only, (E–H) *S. aureus* only, (I–L) *S. aureus* labeled with C-dots, (M–P) *E. coli* only, and (Q–T) *E. coli* labeled with C-dots under a bright field; $\lambda_{\text{ex}} = 330\text{--}380\text{ nm}$, $\lambda_{\text{ex}} = 450\text{--}490\text{ nm}$, and $\lambda_{\text{ex}} = 510\text{--}560\text{ nm}$. The exposure time was 100 ms. The scale bar is 10 μm . Reproduced with permission from Baig et al. Copyright Elsevier, 2017.

Yang et al. synthesized CNDs by autoclaving a solution of glycerol and 3-[2-(2-aminoethyl amino) ethylamino] propyl-trimethoxysilane for 12 h at 260 $^{\circ}\text{C}$ [35]. Next, they functionalized the produced CNDs with quaternary ammonium lauryl betaine, so as to develop positively charged moieties on the surface of the CNDs. The potential of the positively charged, functionalized CNDs for bacterial labeling was examined on three Gram-positive species (*S. aureus*, *Micrococcus luteus*, and *Bacillus subtilis*) and three Gram-negative species (*E. coli*, *P. aeruginosa*, and *Proteusbacillus vulgaris*). The results showed that the CNDs can efficiently label the Gram-positive species, whereas none of the Gram-negative species was labeled. The CNDs can be used to distinguish Gram-positive from Gram-negative species. The difference was attributed to the differences between the cell wall structures and composition. The thick layer of peptidoglycan in the cell membrane of Gram-positive species bears many anionic moieties. As a consequence, electrostatic interactions between the positively charged CNDs and the anion species are favored. In a similar study, Nandi et al. prepared amphiphilic CNDs by carbonizing the 6-O-acylated fatty acid ester of D-glucose [36]. These CNDs can successfully label both Gram-positive

and -negative species (*E. coli*, *P. aeruginosa*, *Salmonella typhimurium*, and *Bacillus cereus*). During the study, while pinpointing the optimal amount of CNDs for the bacteria staining, the authors noticed that each species required a different amount to achieve maximum PL intensity, under a microscope. This was attributed to the different composition of cell membranes, in terms of lipid composition, macroscopic structure and molecular organization. Taking advantage of this phenomenon, the CNDs can be used to distinguish between the different strains by recording the PL intensity and spectral shifts. Additionally, cell division can also be more easily visualized with the CNDs, owing to the high affinity of the CNDs for the cell membrane.

In a different concept, Lu et al. developed nitrogen and phosphorus codoped CNDs from ethylenediamine and yeast extract [37]. These CNDs were negatively charged and, as a consequence of the electrostatic repulsions between them and the negatively charged lipopolysaccharides on *E. coli* membrane, they cannot label the bacteria. However, when the bacteria are killed, their membrane integrity is lost and the CNDs can enter the dead bacteria, making possible their labeling. This can serve as a fast alternative to assess bacteria mortality after exposure to a substance, instead of the plate counting method. In a similar manner, Song et al. developed CNDs from yeast extract and obtained nitrogen, phosphorus, and sulfur codoped carbon dots [38]. The CNDs can efficiently label both Gram-positive and negative dead bacteria (*E. coli* and *Bacillus aryabhatai*), capitalizing on the highly negative charge of the CNDs. Hua et al. prepared two different kinds of CNDs, one from the hydrothermal treatment of *S. aureus* and the other from *E. coli* cells [39]. The CNDs were used for labeling a wide variety of bacteria, including *S. aureus*, *Micrococcus luteus* and *B. subtilis*, *E. coli*, *Proteus bacillus vulgaris*, and *P. aeruginosa*. In addition, the authors showed that the concept of dead cell staining could also be applied to fungal cells by performing relevant experiments on *Saccharomyces cerevisiae* and *Trichoderma reesei*. The above labeling procedure took 1 h to be completed. In an effort to widen the applicability of CNDs labeling potential, three more studies were published, dealing with the labeling of live bacteria and fungi [40–42]. The CNDs were synthesized from different fruits (i.e., carica papaya juice, *Punica granatum* (pomegranate), and *Manilkara zapota* fruits) and their QYs were close to 8%. The CNDs from *Manilkara zapota* fruits required 24 h of incubation with the bacteria or fungi, in order to label them. On the contrary, the other two CNDs can label bacteria and fungi in only 10 min, making the whole process very fast.

According to all the above studies, it can be concluded that imaging of bacteria is not as easy a task as it may sound. This is because many parameters can affect the final outcome. Probably, the most important parameter is the surface charge of the CNDs, which makes possible either the live or the dead cell imaging. The second parameter is the structural characteristics of the cellular membrane that differ among bacteria and grant them different properties. Finally, the different metabolic pathways and metabolome that each cell species has, results in variations in the intensity of the imaging.

4. Imaging Applications for Eukaryotic Cells

Aside from bacterial cells, the potential of CNDs for imaging applications has also been exploited in mammalian cells. As a matter of fact, imaging of mammalian cells is one of the most commonly exploited and overemphasized applications of CNDs. This is because most of the synthesized CNDs fulfill the minimum requirements for a compound to function as an imaging agent. They exhibit a low cytotoxicity, stable fluorescent signal and they do not cause adverse effects on cell physiology [43]. The number of works that revolve around cell imaging is very large and therefore, it would not be prudent or practical to mention all individual works. A list including many characteristics of the various developed CNDs can be seen in Table 1. Our research group has synthesized CNDs from citrus fruits peels (*Citrus sinensis* and *Citrus limon*) or apple seeds and utilized them for the imaging of A549, HeLa, MDA-MB-231, and HEK-293 cells [14,15]. Following different synthetic routes, we prepared CNDs from human fingernails [16,17]. The synthesized CNDs exhibit different PL properties. The derived from microwave treatment with sulfuric acid exhibit an emission at 380 nm, while those from pyrolysis exhibit a dual-emission at 380 and 450 nm. Aside from the different PL properties, the

CNDs differ in the QY (81.4% from pyrolysis and 42.8% with microwave treatment). Both CNDs can efficiently label four different cell lines (Figure 2). Moreover, the CNDs from pyrolysis can promote cell proliferation of HEK-293 cells by up to 18% after 48 h of incubation with $800 \mu\text{g mL}^{-1}$. These findings were so significant that more advanced clinical–biochemical applications can be developed. Du et al. produced CNDs from the hydrothermal treatment of glucose and glycine [44]. The CNDs can effectively label Sh-y5y and MTEC1 cells, as evidenced by confocal microscopy images. The CNDs were localized in the cytoplasm and cell membrane, whereas the PL of the nucleus was very weak. Pal et al. developed polyethyleneimine-passivated CNDs from the hydrothermal treatment of curcumin and polyethyleneimine [31]. Besides the bacterial imaging that these CNDs exhibited (as mentioned above), the authors also labeled A549, NIH 3T3, and HCT-15 cells and achieved multicolor PL. However, differences in the PL intensity were recorded in all cases. Cancer cells A549 and HCT-15 exhibited higher PL compared to fibroblasts NIH 3T3. This was due to the increased metabolic rate and cellular uptake that cancer cells exhibit. In another study, Karakocak et al. produced CNDs by microwave treating a mixture of citric acid and ethylenediamine [45]. The CNDs exhibited excitation-dependent, red PL, which was useful for the multicolor PL labeling of retinal and lens epithelial cells and CHO cells. Moreover, the red PL was particularly useful since cells were able to emit it when excited at 635 nm. This way, the autofluorescence was minimized and the signal-to-background ratio was increased. Xu et al. produced CNDs after microwave treatment of an aspirin–hydrazine mixture [46]. The synthesized CNDs were used for the imaging of RAW246.7, HeLa, KB, and BMSC cells. It is noteworthy that, in this case, the CNDs can enter the cell nucleus and label it alongside with the cytoplasmic area. In another study, CNDs produced from histidine were able to enter cell nucleus of AD-293 cells [6]. Similarly, Wen et al. utilized CNDs from cotton to label both cell nucleus and cytoplasm of A193 cells [18].

Table 1. Representative studies dealing with the synthesis of novel carbon nanodots (CNDs) and their application to eukaryotic cell imaging.

Source	Synthesis Method ¹	$\lambda_{ex}/\lambda_{em}$ (nm)	Type of cells	Reference
Histidine	M: 200 °C, 1 h	360/439	AD-293	[6]
Curcumin and polyethyleneimine	S: 200 °C, 12 h	340/450	A549, NIH 3T3 and HCT-15	[31]
<i>Citrus sinensis</i> or <i>Citrus limon</i>	P: 180 °C, 2 h	365/455 or 330/390–435 (dual emission)	A549, HeLa, MDA-MB-231, and HEK-293	[15]
Apple seeds	P: 250 °C, 3 h	290–340/380–415 (dual emission)	A549, HeLa, MDA-MB-231 and HEK-293	[14]
Human fingernails and sulfuric acid	M:400 W, 2 min	320/380	A549, HeLa, MDA-MB-231, and HEK-293	[16]
Human fingernails	P: 200 °C, 3 h	330–370/380–450 (dual emission)	A549, HeLa, MDA-MB-231 and HEK-293	[17]
Glucose and glycine	S: 180 °C, 6 h	370/475	Sh-y5y and MTEC1	[44]
Citric acid and ethylenediamine	M:1100 W, 88 s	540/600	Retinal epithelial, lens epithelial and CHO cells	[45]
Aspirin and hydrazine	M:500 W, 8 min	360/432	RAW246.7, HeLa, KB, and BMSC	[46]
Cotton	P: 300 °C, 2 h	330/460	A193	[18]
L-citrulline	S: 220 °C, 12 h	350/450	HeLa	[19]
Coriander leaves	S: 240 °C, 4 h	320/400	A549, L-132	[20]
Ginsenoside Re, citric acid, and ethylenediamine	S: 200 °C, 10 h	360/460	A375	[47]
Cellulolytic enzyme lignin	6 h stirring in ethanol	280/390	HeLa	[48]
Kidney beans	P: 450 °C, 2 h	340/460	HeLa	[49]
Citric acid and tris(hydroxymethyl) methylaminomethane	S: 250 °C, 6 h	330/420	MCF-7	[22]
L-glutamic acid and silica gel	M:640 W, 5 min	370/450	BT-474	[50]
Citric acid and ethylenediamine	M:600 W, 13 min	366/488	HepG2	[51]

Table 1. Cont.

Source	Synthesis Method ¹	$\lambda_{ex}/\lambda_{em}$ (nm)	Type of cells	Reference
Citric acid, sodium nitrate, and potassium nitrate	P: 220 °C, 6 h	330/440	HeLa	[52]
Citric acid, urea, and sodium fluoride	M:750 W, 5 min	530/600	C6 glioma cells	[53]
Citric acid, ethylenediamine, and alkali lignin	S: 150 °C, 4 h	377/454	HeLa	[54]
Alanine and ethylenediamine	S: 200 °C, 6 h	320/390	MCF-7	[55]
3-Bromophenol	S: 170 °C, 8 h	318/430	HeLa	[56]
Peach extract and ammonia	S: 180 °C, 5 h	325/404	MDA-MB-231	[57]
Boric acid and sucrose	S: 180 °C, 10 h	365/450	HeLa	[58]
Dextrin and sulfuric acid	M:800 W, 2.5 min	440/486	MDA-MB-231	[59]
Cyclodextrin, sulfuric acid, and ethylenediamine	stirring 2 h at 90 °C	390/510	H1299	[60]
Carrot juice	S: 160 °C, 6 h	360/442	HaCaT	[21]
Adenosine-5'-triphosphate	S: 180 °C, 10 h	340/440	A549	[61]
Phthalic acid and triethylenediamine	M:700 W, 1 min	360/500	HeLa	[62]
Citric acid and polyethyleneimine	S: 180 °C, 20 h	420/460	CAL-27	[63]
Polyethyleneimine and nitric acid	reflux at 120 °C for 72 h	320/420	HeLa	[23]
Sucrose and phosphoric acid	M:100 W, 3 min and 40 s	225/453	red blood cells	[64]
N-(β -aminoethyl)- γ -aminopropyl methyl dimethoxy silane and citric acid	heating at 240 °C for 1 min	340/450	BGC823	[65]
Glycerol and 4,7,10-trioxa-1,13-tridecanediamine	M:700 W, 10 min	340/450	HepG-2	[27]

¹ S: solvothermal; M: microwave-assisted; P: pyrolysis.

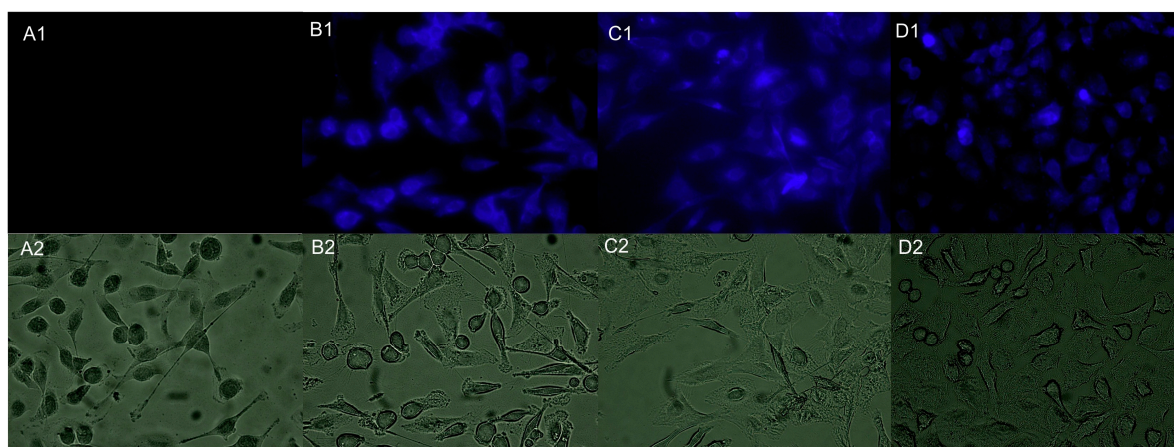


Figure 2. Fluorescence microscopy images of (A) non-treated and CNDs-treated (B) MDA-MB-231, (C) A549, (D) HeLa under UV (1), and visible (2) light. Reproduced with permission from Chatzimitakos et al. Sens. Actuators B 2018. Copyright Elsevier, 2018.

Li et al. synthesized CNDs using an alternative pyrolysis method by incorporating citric acid in a eutectic mixture of salts [52]. The low-cytotoxicity CNDs were used for the efficient multicolor imaging of HeLa cells. Moreover, the CNDs were used as chelating agents for gadolinium ions. Generally, gadolinium ions are excellent factors for magnetic resonance imaging applications; however, their toxicity hinders their applicability. The gadolinium–CNDs complex was nontoxic to HeLa cells, after 48 h of incubation, at a concentration of 1.2 mg mL^{-1} . Hence, the complex was able to label HeLa cells at different excitation wavelengths, just like the plain CNDs. Moreover, the authors found that the PL intensity of the cells decreased as the incubation time with the gadolinium–CNDs complex increased, suggesting practical applicability in both magnetic resonance imaging and fluorescence imaging techniques. Yang et al. synthesized CNDs codoped with nitrogen and fluoride [53]. Because

of the electron withdrawing nature of the fluoride atoms, the synthesized CNDs exhibited red PL, attributed to the narrower energy gap of $\pi-\pi^*$ transitions, compared to CNDs without fluoride. The red PL is useful because it causes less adverse effects on cells and, as a consequence, to tissues, while it also achieves higher penetration. According to the above, the synthesized CNDs were used for the imaging of C6 cells, at an excitation wavelength of 530 nm. In another study, Loukanov et al. developed an approach to quantify the concentration of CNDs in real-time monitored tobacco BY-2 cells [66]. To do so, they first prepared a calibration curve for the relative emission intensity and the concentration of the CNDs using liposomes that they prepared with surfactants. Then, they measured the natural autofluorescence noise of nonlabeled cells and subtracted this number from the PL emitted by labeled cells. Using the calibration curve they were able to calculate the amount of CNDs in the cells.

Shakhov et al. published a radically different concept of cell labeling with CNDs [67]. Instead of adding a fixed amount of CNDs to the growth medium of the cells, they produced the CNDs inside the cells, *in situ*. In their work, they used Mouse GV oocytes and they demonstrated that during oocyte maturation they can produce CNDs inside the cells to track the reorganization of the cellular structure, the cell cycle and the transport of intracellular material. To produce the CNDs, they used NIR femtosecond laser pulses in order to generate low-density electron plasma and heated a specific area in the cell so that carbonization of organic compounds occurs. Depending on the exposure to the laser pulses, the PL intensity of the produced CNDs, with an optimum emission achieved in only 131 ms. This technique is not dependent on the composition of the target area as validated by targeting three different areas (i.e., nucleolus, nucleus, and cytoplasm). The size of the CNDs was dependent on the laser power. The produced CNDs remained visible for several hours and even up to 24 h after their production. Most importantly, the whole procedure is “friendly” for the cells, since it does not interfere with the normal cell processes and does not cause any cell mortality. The same holds true for the developed CNDs.

5. Target-Specific Imaging Applications for Eukaryotic Cells

There are only few studies about CNDs for imaging of specific cellular targets, in contrast to those described above. Jung et al. prepared zwitterionic CNDs by irradiating with microwaves a solution containing citric acid and beta alanine [68]. The presence of positively charged groups on the CNDs surface mediated the interactions with the negative charges cell membrane. Ultimately, CNDs entered the cytoplasm by passive diffusion and clathrin- and caveolae-mediated pathways. Next, CNDs enter the cell nucleus because their small size facilitates their diffusion through nuclear pore complexes. The whole process is facilitated by the negative charges on the surface of the CNDs and the histone nuclear import-associated process that takes place, according to the relevant experiments. In another study, CNDs from citric acid and polyethylene glycol were prepared [69]. The CNDs alone cannot enter the cell nucleus, as occurs with the majority of the CNDs. To overcome this hindrance, authors functionalized CNDs with a nuclear localization signal peptide. The functionalized CNDs, upon entering the cytoplasm, bind with importin and then localization to cell nucleus takes place.

The cell nucleolus is another target of CNDs. Phenylenediamine and cysteine were subjected to solvothermal treatment and yielded CNDs [70]. Upon incubation of HeLa cells with CNDs, the latter were localized in the nucleoli of the cells. The imaging of cell nucleolus was straightforward since no signs of fluorescence from lysosomes or endosomes were detected, after 5 min of incubation with the CNDs. The imaging of nucleolus was stable for 24 h and the CNDs are not transferred to another area inside the cell. The CNDs were compared with Hoechst 33342 and SYTO RNASelect dyes for imaging of live and fixed cells. As regards live cells, the first dye labels the whole nucleus, without the nucleolus. The second dye can stain neither the nucleolus nor the nucleus. On the other hand, when fixed cells are incubated with the dyes they can both stain nucleolus. The CNDs were effective in this case too. This highlights that the CNDs can be used for imaging of nucleolus, even in cases that commercially available dyes are inefficient. In a similar study, He et al. took advantage of the selectivity of CNDs of higher molecular weight for RNA over DNA and utilized them to label cell

nucleoli, where RNA exists at higher content levels [71]. Fluorescence signals were also recorded in the cytoplasm of cells ascribed to the presence of RNA. However, the lower amount of cytoplasmic RNA made feasible the clear discrimination of nucleolus. The two above studies demonstrate that some CNDs are capable of achieving selective labeling of cells. However, if this is not possible, the surface chemistry of the CNDs makes feasible the functionalization with specific molecules (as can be seen also later on) that render the whole complex selective.

Another targeted labeling was reported by Chen et al. [72]. In their study, they prepared CNDs by heating polyethylene glycol at 160 °C. Then, they functionalized them with goat antimouse IgG. This way, the functionalized CNDs are able to target the microtubules of lung cancer cells (i.e., A549). Compounds with thiol groups, such as galactosyltransferase and protein kinase D can anchor to the Golgi system of a cell [73]. In this context, Yuan et al. developed CNDs from citric acid and penicillamine, which had plenty of free thiol groups. As a consequence, when used for the imaging of Hep-2 cells, the Golgi system was fluorescent, whereas the rest parts of the cell exhibited no fluorescence. To validate the affinity, authors prepared CNDs by replacing penicillamine with alanine. The new CNDs were not selective towards the Golgi system.

Mitochondria have also been the label target of some CNDs [74–77]. In all cases, authors conjugated triphenylphosphonium on the CNDs surface. The positive charges of triphenylphosphonium facilitate the internalization of the CNDs conjugates into the cytoplasm, whereas the even larger membrane potential of mitochondria tends to accumulate the conjugates to the mitochondria [74]. Xu et al. followed the same principle and prepared CNDs for targeting mitochondria [77]. In addition, they added S-nitrosothiol to the triphenylphosphonium-CNDs conjugate. The nitrosothiol can release nitric oxide upon light irradiation. This way, the new conjugate can enter into the cytoplasm, target mitochondria, and act as a carrier for the nitric oxide system so as to damage mitochondria and cause cell apoptosis. Zhang et al. developed magnetic silica nanoparticles with CNDs and triphenylphosphonium [75]. As happened in the above cases, they were able to target only mitochondria. The magnetic core of the nanoparticles increased the cellular uptake of the nanomaterial under a static magnetic field and rendered the imaging process more efficient.

Exosomes were the imaging target of the study of Jiang et al. [78]. They produced gold–CNDs by combining carbon dots and gold nanoclusters, which then they modified with rabbit anti-HER2. The modified CNDs were used as a fluorescent agent to selectively target either extracellular or intracellular cancer-derived exosomes. This way, they can monitor the translocalization of exosomes inside a cell, their excretion from the cell and their internalization by other cells, as part of the genetic information exchange between tumor cells.

Another aspect of targeted cell imaging is the target of molecules inside the cells. Our research group has synthesized CNDs from *Citrus sinensis* peels, which were utilized as a fluorescent probe for the detection of Fe^{3+} ions [15]. Capitalizing on this property of the CNDs, we utilized them for the intracellular detection of Fe^{3+} ions in HeLa cells. Cells incubated in normal growth medium were highly fluorescent, after addition of CNDs. In contrast, cells incubated in a growth medium which contained Fe^{3+} ions (in sublethal doses) exhibited weaker fluorescence after incubation with the CNDs. Similarly, Lu et al. and Chen et al. produced CNDs that can be used for sensing of intracellular Fe^{3+} in HeLa and RAW264.7 cells, respectively [79,80]. Likewise, Kaur et al. produced CNDs from glycerol and ethylenediamine, which they modified with 1,3-disubstituted calix [4] arene to enhance their fluorescence properties [81]. The fluorescence of the developed CNDs can be quenched with the addition of Zn^{2+} ions. As a consequence, the CNDs are used as a fluorescent probe for the detection of this ion in cells. Kong et al. produced CNDs that could be used as a fluorescent probe to detect intracellular Al^{3+} ions in HUVEC cells, based on a Förster resonance energy transfer (FRET) mechanism [82]. A more complex system was developed by Zhang et al. [83]. The fluorescence intensity of the CNDs developed by the authors can be quenched in the presence of Cu^{2+} ions. Thus, the intracellular levels of copper ions can be recorded. In addition to that, the authors found that

the presence of sulfide anions can recover the fluorescence of the quenched CNDs, leading to the development of an “off-on” system.

Intracellular glucose was the target of the aminophenyl boronic acid-functionalized CNDs that Kiran et al. developed [84]. The higher the concentration of the intracellular glucose the lower the intensity of the fluorescence emitted. These CNDs can be used for the monitoring of the changes in the intracellular glucose levels, which can be useful for the diagnosis of glucose-related health issues. Liu et al. developed CNDs whose PL can be quenched in the presence of glutathione [85]. Since glutathione is the molecule that primarily contributes to the intracellular redox state, by visualizing differences in the levels of glutathione in cells conclusions can be drawn for the redox state of the cell and the physiological processes that are regulated based on the redox state. Shi et al. developed a CND-based fluorescent probe that can detect tetracycline in vitro [86]. In a similar manner, cells with low levels of tetracycline exhibit intense PL, and as the concentration of tetracycline increases, the fluorescence emission decreases. It is noteworthy that besides alterations of tetracycline concentration, the PL of the CNDs is sensitive to the temperature. At 25 °C, the cells exhibit an intense green fluorescence, which lessens as the temperature increases to 35 °C. This is a reversible process and as the temperature decreases, cells exhibit more intense fluorescence. These CNDs can be used as an in vitro nanothermometer. A more detailed study was published by Kalytchuk et al. [87]. They prepared CNDs from citric acid and cysteine and used them as a nanothermometer. They conducted an extensive study of many parameters that can affect the fluorescence imaging and they showed that with careful selection, the accuracy of the calculated temperature can reach up to 0.27 °C.

Another type of intracellular fluorescent sensors has been developed for pH measurements. Such sensors have been developed as an alternative to the fluorescent protein-based pH sensors, which are accompanied by some disadvantages [88]. Shangguan et al. produced CNDs from basic fuchsin and citric acid [88]. When the CNDs were added into aqueous solutions with different pH, the PL emission was shifted from 475 nm to 545 nm. In order to develop a fluorescent sensor of intracellular pH, the authors firstly prepared a ratiometric calibration curve using HeLa cells which were incubated in HEPES-buffered solution containing nigericin. Then, in another cell culture, they added molecules with well-known pH changing abilities for cells, such as chloroquine or dexamethasone, and observed the different fluorescence. From the fluorescence intensity at the two aforementioned wavelengths, and by using the ratiometric calibration curve, they calculated the pH of the cell, besides observing the different color of the cells. Likewise, Chandra et al. developed CNDs from the mushroom *Agaricus bisporus* and ethylenediamine and they found that the CNDs can detect changes in the intracellular pH of HeLa cells [89]. Their CNDs exhibit dual emission, one at 450 nm and one at 550 nm. Of the two emission maxima, the first was found to be independent of the pH changes, whereas the intensity of the second peak was altered at different pH values. Examining intracellular pH using such dots is more accurate and reliable, according to the authors, since there is a pH-independent peak, which can act as a calibration standard to correct for any interactions between CNDs and intracellular components.

A more complex approach was employed from Du et al., who treated hydrothermally a mixture of glycerin and 2,2'-(Ethylenedioxy)bis(ethylamine) to yield CNDs [76]. Next, the CNDs were modified with triphenylphosphonium so that they could be selective towards cell mitochondria. Then, a hydrogen peroxide recognition element (i.e., 3-Oxo-3',6'-bis(4,4,5,5-tetramethyl-1,3,2-dioxaborolan-2-yl)-3H-spiro [isobenzofuran-1,9'-xanthene]-6-carboxylic acid), based on Förster resonance energy transfer (FRET), was also attached on the surface of the modified CNDs. When cells are incubated with the CNDs complex, their mitochondria are labeled and a blue fluorescence can be seen, while green fluorescence can scarcely be seen. Upon addition of hydrogen peroxide to cells, the blue fluorescence is quenched and the green fluorescence is increased, due to FRET. The above highlights the applicability of the CND-based complex as a ratiometric fluorescent imaging agent for targeted endogenous and exogenous hydrogen peroxide in living cells. In another study, Zholobak et al. prepared CNDs by melting citric acid and urea [90]. They incubated diploid epithelial swine testicular cells with the CNDs and found that although the CNDs cause no toxicity to the cells, they inhibit the activity of NADP-H-dependent

oxidoreductase enzymes. Moreover, fluorescence emitted by cells was relatively weak. However, when hydrogen peroxide was added, cells were subjected to oxidative stress and CNDs fluorescence was more intense. Interestingly, the fluorescence is not uniform and areas of higher and lower intensity could be observed. Higher fluorescence could be seen at mitochondria around the nucleus and at the nucleolus, which try to form ribosomes and proteins to counteract the oxidative stress. Overall, these CNDs can be used to discriminate normal cells from cells that are subjected to oxidative stress and monitor the concentration of hydrogen peroxide in cells.

One of the most fascinating applications of CNDs in targeted imaging is the selective cell imaging. More specifically, CNDs can selectively and more readily label cancer cells that usually overexpress folate receptors, over cells with fewer folate receptors. In this context, Liu et al. and Bhunia et al. prepared CNDs from hydrothermal treatment of folic acid [91,92]. The residues of folic acid on the surface of the synthesized CNDs make them perfect molecules for binding at folate receptors. As a proof of concept, the authors used HeLa cells that overexpress folate receptors, and found that they exhibit strong fluorescence after exposure with the CNDs. The same observation was recorded for SKOV3 cells, which also have plenty of folate receptors. When A549 cells were used, their fluorescence was weak, which was expected since they have a deficiency of folate receptors. Bhunia et al. examined this concept in HepG2 and MCF7 cells in addition to the aforementioned cell lines and found that these cells exhibited moderate fluorescence, which is in accordance with their folate receptor expression. Even in the cases that CNDs do not bear inherent properties for direct selectivity of a target cell, their surface chemistry makes functionalization with other molecules an easy task and lights up the way for more advanced applications. This way, Wang et al. produced CNDs from tryptophan and phenylalanine and then they modified them with the MUC-1 aptamer [93]. This way the modified CNDs can easily bind to the MUC-1 glycoprotein (an important cancer biomarker in the case of human epithelial cancer). The concept was proved using MCF-7 and HepG2 cells, with the first solely exhibiting fluorescent, owing to their overexpressed MUC-1 and the latter not being labeled. Motaghi et al. developed a similar concept as the one described above [94]. The CNDs were conjugated to AS1411 aptamer and their fluorescence was quenched. This aptamer binds to nucleolin, which is in abundance in cancer cells. When cancer cells that overexpress nucleolin are incubated with the nonfluorescent conjugate the aptamer is released from the CNDs and binds to nucleolin. As a result, the PL of the CNDs is recovered and this can be monitored to separate cancer cells from normal cells or from cells that do not overexpress nucleolin. The above studies highlight the tremendous potential of CNDs in the development of noninvasive imaging applications for the diagnosis of cancer.

6. In Vivo Imaging Applications

As it would be expected, after having developed fluorescent labeling techniques for prokaryotes and eukaryotes, the research interest was focused on applying CNDs for fluorescent labeling of small animals. The successful application of CNDs in vivo has its limitations, which need to be overcome. The toxicity, blood compatibility, rapid excretion from the body, suitable hydrodynamic diameter, and the lowest possible adsorption of proteins must be taken into account [43]. Another parameter which must be carefully considered is the excitation/emission wavelength, because the light can be scattered due to the Rayleigh scattering effect in the tissue and results in a high background signal [95]. The first study to present the feasibility of CNDs for in vivo imaging was published in 2009 by Yang et al. [96]. They carried out subdermal or intravenous injections of polyethylene glycol-functionalized CNDs solution in mice. With regard to the subdermal injection, the injected area exhibited high fluorescence, which faded nearly 24 h after injection, since the rate of CNDs diffusion was low. When CNDs was injected intravenously, fluorescence was observed only in the bladder area. Moreover, after 3 h, CNDs could be detected in the urine. After 4 h, the organs were analyzed ex vivo and it was found that the kidneys were fluorescent whereas the liver was not. All of the above corroborate excretion of the CNDs through urine when injected intravenously. Similar results were observed by Xu et al. and

Kuo et al. who examined the imaging potential of CNDs from aspirin and from polyvinylpyrrolidone and glycine, respectively, on mice [46,97].

In another study, Yang et al. produced fluoride-doped CNDs that exhibit red fluorescence capable of penetrating deeply, with less adverse effects [53]. They injected intravenously a CNDs solution in mice with xenograft tumor and found that the CNDs entered successfully the blood circulation. It is noteworthy that after 12 h, the CNDs were localized in the tumor area, which exhibited stronger fluorescence (Figure 3). Since no adverse health effects were observed in the animals, the proposed CNDs are an excellent fluorescent probe for tumor diagnosis. Zheng et al. produced CNDs using glucose and aspartic acid [98]. From in vitro experiments, it is evident that the CNDs are more selective towards the C6 cells than noncancerous L929 cells. Authors took advantage of this selectivity and injected the CNDs in the tail vein of orthotopic C6 glioma-bearing mice. Interestingly, the CNDs can freely penetrate the blood–brain barrier and reach the brain in only 5 min, while in 15 min the highest fluorescence could be observed only from the glioma tissue, with the normal brain tissue to scarcely exhibit fluorescence. Similarly, Ren et al. produced red emissive CNDs from the hydrothermal treatment of phenylpropionic acid polymers [99]. Next, they prepared liposomes loaded with the CNDs, and authors demonstrated that the CNDs loaded liposomes are more efficient for the MCF-7 tumor imaging in nude mice, compared with plain CNDs (Figure 4).

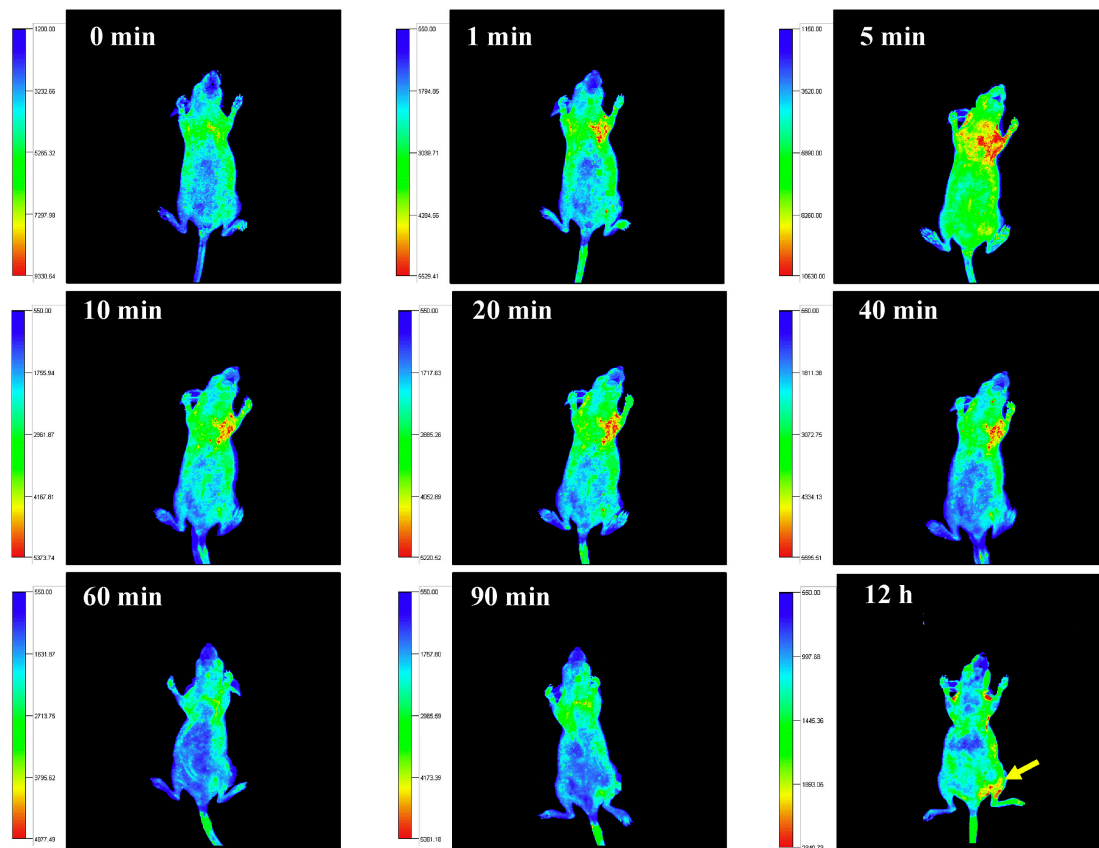


Figure 3. In vivo fluorescent images of nude mouse bearing xenograft tumor before and after i.v. injection of CDs at different time points. Reproduced with permission from Yang, et al., Carbon 2018. Copyright Elsevier, 2018.

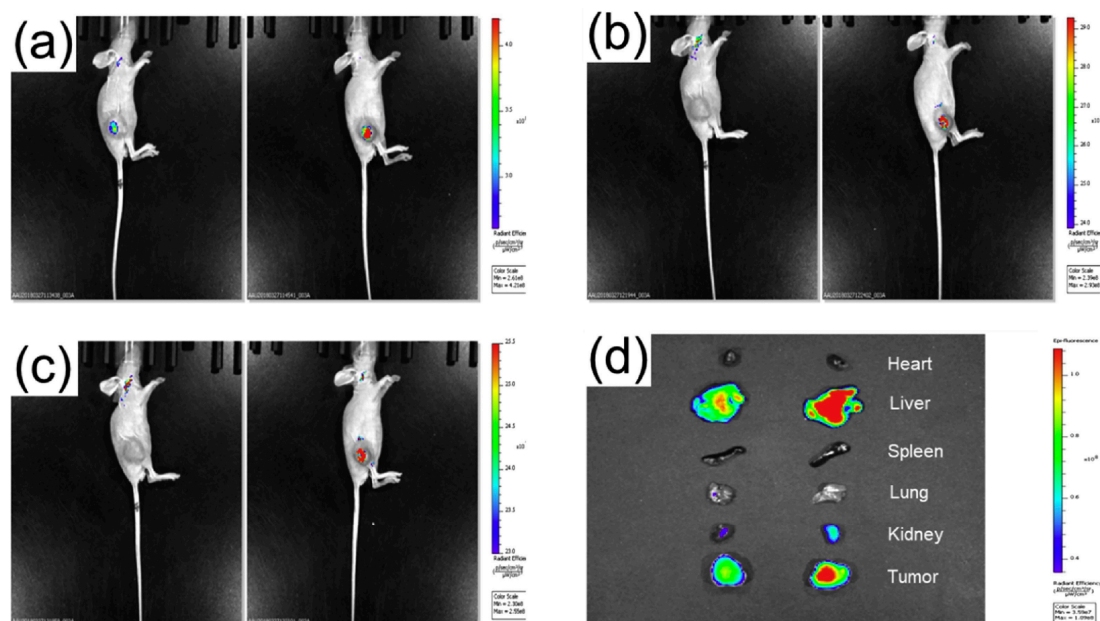


Figure 4. (a–c) In vivo photoluminescence (PL) images of nude mice treated with intratumoral injection of CDs (the left) and CDs + CB liposomes (the right) 0.25 h, 1 h, and 2 h postinjection, respectively. (d) Ex vivo images of mice tissues 24 h post tail intravenous injection of CDs (the left) and CDs + CB liposomes (the right). The color bars represent the PL intensity. Reproduced with permission from Ren et al. Copyright Elsevier, 2019.

In their study, Hua et al. intravenously injected U14 tumor-bearing mice with CNDs conjugated with protoporphyrin IX [70]. The results showed that the CNDs are accumulated in the tumor area, 6 h after the injection. Ex vivo experiments validated that the CNDs are localized in the tumor area 24 h after injection, while in the following days the CNDs are found mostly in the kidneys, bespeaking liver and kidney clearance. Considering the nucleus-targeting ability of the CNDs, the authors showed that the conjugated CNDs can efficiently be used in photodynamic therapy of the tumor, without causing damage to other organs or tissues of the animal. Similarly, Lan et al. produced sulfur and selenium codoped CNDs by treating hydrothermally an alkaline solution of polythiophene and diphenyl diselenide [100]. When the CNDs were injected into healthy mice no adverse health effects were observed, thus proving good biocompatibility of the CNDs. When the CNDs were injected into a tumor, the latter became highly fluorescent, making its visualization easy. The developed CNDs were used, also, for the photothermal therapy of mice with subcutaneous 4T1 murine breast cancer cells. The authors found that after 6 min of irradiation the temperature of the tumor that was injected with CNDs increased to 52 °C, compared with the temperature of 42 °C that the tumor of the control group reached. This increase significantly inhibits the growth of tumor cells. Altogether, the two above studies highlight the tremendous potential of CNDs to be used not only for diagnosis purposes, but also for specific treatments.

Another interesting and conceptually different work was presented by Zhang et al. [101]. The authors prepared CNDs doped with either tellurium or selenium. Both kinds of CNDs, owing to the redox properties of the metal, in the presence of the superoxide anion were oxidized and their fluorescence signal significantly increased. In the presence of glutathione the fluorescence was quenched since the oxidized CNDs returned to their original state. This ability of the doped CNDs was put forward for the separation of cancer cells from normal cells, since the first contain higher concentration of superoxide anions. In addition to the above, the CNDs were applied in the abdomen tissue of healthy mice and the breast tumor tissue of mice. In the last case, the observed fluorescence was much higher compared to the first case, owing to the aforementioned reason. The tellurium-doped CNDs exhibited excellent sensitivity for the superoxide anions (limit of detection = 8.0 pM) making

it possible for them to monitor superoxide anions. The authors found that after intense exercise or emotional changes, such as irritability from noise or depression, the levels of superoxide anions change. This change could easily be observed with the developed fluorescent probe. Thus, a new imaging tool was developed for the reactive oxygen species-mediated health conditions.

Besides mice, CNDs have been used for the imaging of zebrafish. Pal et al. examined the potential of CNDs for imaging applications in zebrafish embryos [31]. The authors found that even a low content of CNDs (i.e., $0.4 \mu\text{g mL}^{-1}$) can efficiently label the embryos. CNDs could easily pass the chorionic membrane and they were accumulated in the yolk sac region. Wei et al. incubated zebrafish embryos with nitrogen-doped CNDs, boronic acid-functionalized nitrogen-doped CNDs, and phenylboronic acid-functionalized nitrogen-doped CNDs and examined the fluorescence after 72 h postfertilization [102]. They found that the phenylboronic acid functionalized CNDs were toxic for the embryos, since they killed all of them in 9 h. With regard the other two CNDs species, in the first 48 h they were localized mainly in the chorions and they did not affect the normal growth of the embryos. The fluorescence intensity decreases as time passes (i.e., from 2 to 72 h postfertilization) but the hatched larvae are fluorescent. Similar observations were carried out by Kang et al., who attributed the lower fluorescence of the embryos as time passes to excretion from the digestive system [103]. In their study, they used two ways to expose the embryos to CNDs: the soaking and microinjection. They found that with each method, different distribution of the CNDs (produced by glycine and ethylenediamine) is achieved in the embryos, knowledge that can be utilized in the development of different applications. In addition to the embryos, they also examined the imaging of larvae exposed to CNDs. They found that the CNDs enter zebrafish larvae by skin absorption and swallowing. The dorsal aorta, eye lens, and intestine were highly fluorescent, meaning that the CNDs can enter circulatory system, the eye (via the blood–ocular barrier) and the digestive system, respectively. The above exhibit the tissue-dependent distribution of the CNDs in the larvae. Moreover, authors found that the CNDs cannot pass the blood–brain barrier, leading to safer imaging applications (in terms of cerebral injury). This inability of the CNDs to pass the blood–brain barrier can limit their application in studies of the central nervous system [104]. To overcome this hindrance, Li et al. developed 5-(aminomethyl) fluorescein–transferrin–CNDs conjugates [104]. Bare CNDs could not enter the blood–brain barrier, despite their small size. Therefore, the authors added transferrin to target the transferrin receptors and make easier the penetration of the CNDs. Owing to the low PL of the CNDs–transferrin conjugate, no signal could be observed under fluorescence microscope. Therefore, they added the fluorescent dye to enhance the signal. This conjugate can efficiently surpass the limitation of passing the blood–brain barrier and can be used in applications that other CNDs cannot. Wei et al. also examined the potential of CNDs to be used for imaging of zebrafish embryos and larvae [105]. Interestingly, they found that when larvae were exposed successively to CNDs and hydrogen peroxide, their content in reactive oxygen species and malondialdehyde was significantly lower, compared with the control larvae. To examine the decrease of reactive oxygen species, authors studied the expression of some relevant genes. Interestingly, they found that the mRNA of some genes was increased, owing to the upregulation of the relevant genes by the CNDs. In another concept, Li et al. injected zebrafish larvae with CNDs [106]. The CNDs employed exhibited very low PL, owing to their low QY. However, 30 min after postinjection, strong PL was observed in the skeletal structures. The fluorescence of the skeletal structure can be retained even after eight days postinjection. Among the different skeletal tissues, the CNDs were targeting more selectively the calcified bones. This is a novel type of fluorescence imaging agent for calcified bones, since in most cases, targeting of bones is difficult, owing to the fact that bones are surrounded by soft tissue and interactions with it are difficult to avoid.

Lastly, Saxena et al. [107] incubated larvae mosquitoes (i.e., *Anopheles* sp., *Aedes* sp., and *Culex* sp.) with CNDs and they observed their growth during a 30-day period. Besides the excellent imaging performance of the CNDs in this animal species, the authors made some interesting observations. At a concentration of 3 mg mL^{-1} , the CNDs are not toxic for the mosquito species, however, they can halt the adulthood of the mosquitoes. This was attributed to the disruption of normal hormone activity.

However, they found that this is a reversible phenomenon, since the mosquitoes, whose adulthood is halted when exposed to fresh water (without containing CNDs), continued to grow up in parallel with the excretion of CNDs from their body.

7. Conclusions and Future Perspectives

Undoubtedly, CNDs have given a new, strong impetus to physical and life sciences for the following reasons. (1) The cost of producing CNDs is very low and the versatility of the synthetic procedures and the final product is very high; (2) CNDs are one of the few classes of nanomaterials with inherent fluorescence properties; (3) the presence of multiple functional groups on their surface render them a unique material that can overcome many hindrances that other nanomaterials face, such as water dispersibility; and (4) their carbon-based core makes them less toxic for living organisms, compared with the heavy metal-based quantum dots. Apart from the sensing applications of CNDs, their excellent PL was utilized for in vitro and in vivo imaging applications. Several research groups have exploited the potential of the CNDs to label bacteria (Gram-positive and/or Gram negative and live or dead bacteria), fungi, eukaryotic cells (mammalian and plant cells), and animals (mice, zebrafish, and mosquitoes). These efforts resulted in the advancement of the basic research in this field. It was not until recently that more advanced and sophisticated imaging variants have been developed, based on the functionalization of the CNDs with various molecules (aptamers, antibodies, polyethylene glycol, etc.). This way, selective imaging of cancer cells over noncancerous cells and tumor tissue over normal tissue were achieved. Moreover, biosensing applications have been developed, aiming to detect molecules of biological importance, such as reactive oxygen species, metal ions, and RNA, in real-time conditions inside cells, in order to monitor alterations of their levels and draw conclusions on abnormal conditions or even track mood changes in animals.

As it can be seen from this literature review, much work has been made towards the application of CNDs in imaging applications. However, still many challenges have to be faced. First of all, the PL of the CNDs should be tuned to wavelengths higher than blue and green, such as deep red and near-infrared. Moreover, their structural characteristics must be elucidated depending on their synthesis methods in order to exploit their full in bioimaging. From the studies discussed herein it can be seen the precursor materials along with the synthesis method can result in CNDs with radically different targeted imaging properties. Finally, more molecules should be examined for the functionalization of CNDs in order to develop new fascinating imaging applications and render CNDs suitable for more imaging techniques, such as photoacoustic and magnetic resonance imaging. All in all, the best is yet to come.

Author Contributions: Conceptualization, A.K., T.C. and C.S.; Investigation and Writing-Original Draft Preparation, A.K.; Visualization, T.C.; Writing-Review & Editing, A.K., T.C., C.S.

Funding: This research received no external funding.

Conflicts of Interest: The authors declare no conflicts of interest.

References

1. Salata, O. Applications of nanoparticles in biology and medicine. *J. Nanobiotechnol.* **2004**, *2*, 3. [[CrossRef](#)] [[PubMed](#)]
2. Baker, S.; Baker, G. Luminescent carbon nanodots: Emergent nanolights. *Angew. Chem. Int. Ed.* **2010**, *49*, 6726–6744. [[CrossRef](#)] [[PubMed](#)]
3. Wang, R.; Lu, K.; Tang, Z.; Xu, Y. Recent progress in carbon quantum dots: Synthesis, properties and applications in photocatalysis. *J. Mater. Chem. A* **2017**, *5*, 3717–3734. [[CrossRef](#)]
4. Du, F.; Zeng, F.; Ming, Y.; Wu, S. Carbon dots-based fluorescent probes for sensitive and selective detection of iodide. *Microchim. Acta* **2013**, *180*, 453–460. [[CrossRef](#)]
5. Yang, K.; Liu, M.; Wang, Y.; Wang, S.; Miao, H.; Yang, L.; Yang, X. Carbon dots derived from fungus for sensing hyaluronic acid and hyaluronidase. *Sens. Actuators B* **2017**, *251*, 503–508. [[CrossRef](#)]

6. Huang, H.; Li, C.; Zhu, S.; Wang, H.; Chen, C.; Wang, Z.; Bai, T.; Shi, Z.; Feng, S. Histidine-derived nontoxic nitrogen-doped carbon dots for sensing and bioimaging applications. *Langmuir* **2014**, *30*, 13542–13548. [[CrossRef](#)]
7. Wang, Y.; Hu, A. Carbon quantum dots: Synthesis, properties and applications. *J. Mater. Chem. C* **2014**, *2*, 6921–6939. [[CrossRef](#)]
8. Roy, A.; Kim, S.; Paoprasert, P.; Park, S.; In, I. Preparation of biocompatible and antibacterial carbon quantum dots derived from resorcinol and formaldehyde spheres. *RSC Adv.* **2015**, *5*, 31677–31682. [[CrossRef](#)]
9. Su, X.; Xu, Y.; Che, Y.; Liao, X.; Jiang, Y. A type of novel fluorescent magnetic carbon quantum dots for cells imaging and detection. *J. Biomed. Mater. Res. A* **2015**, *103*, 3956–3964. [[CrossRef](#)]
10. Matea, C.; Mocan, T.; Tabaran, F.; Pop, T.; Mosteanu, O.; Puia, C.; Iancu, C.; Mocan, L. Quantum dots in imaging, drug delivery and sensor applications. *Int. J. Nanomed.* **2017**, *12*, 5421–5431. [[CrossRef](#)]
11. Wu, Y.; Wu, H.; Kuan, C.; Lin, C.; Wang, L.; Chang, C.; Wang, T. Multi-functionalized carbon dots as theranostic nanoagent for gene delivery in lung cancer therapy. *Sci. Rep.* **2016**, *6*, 21170. [[CrossRef](#)]
12. Hassan, M.; Gomes, V.; Dehghani, A.; Ardekani, S. Engineering carbon quantum dots for photomediated theranostics. *Nano Res.* **2018**, *11*, 1–41. [[CrossRef](#)]
13. Sharma, V.; Tiwari, P.; Mobin, S. Sustainable carbon-dots: Recent advances in green carbon dots for sensing and bioimaging. *J. Mater. Chem. B* **2017**, *5*, 8904–8924. [[CrossRef](#)]
14. Chatzimarkou, A.; Chatzimitakos, T.; Kasouni, A.; Sygellou, L.; Avgeropoulos, A.; Stalikas, C. Selective FRET-based sensing of 4-nitrophenol and cell imaging capitalizing on the fluorescent properties of carbon nanodots from apple seeds. *Sens. Actuators B* **2018**, *258*, 1152–1160. [[CrossRef](#)]
15. Chatzimitakos, T.; Kasouni, A.; Sygellou, L.; Avgeropoulos, A.; Troganis, A.; Stalikas, C. Two of a kind but different: Luminescent carbon quantum dots from Citrus peels for iron and tartrazine sensing and cell imaging. *Talanta* **2017**, *175*, 305–312. [[CrossRef](#)] [[PubMed](#)]
16. Chatzimitakos, T.; Kasouni, A.; Sygellou, L.; Leonardos, I.; Troganis, A.; Stalikas, C. Human fingernails as an intriguing precursor for the synthesis of nitrogen and sulfur-doped carbon dots with strong fluorescent properties: Analytical and bioimaging applications. *Sens. Actuators B* **2018**, *267*, 494–501. [[CrossRef](#)]
17. Chatzimitakos, T.; Kasouni, A.; Troganis, A.; Stalikas, C. Carbonization of human fingernails: Toward the sustainable production of multifunctional nitrogen and sulfur codoped carbon nanodots with highly luminescent probing and cell proliferative/migration properties. *ACS Appl. Mater. Interfaces* **2018**, *10*, 16024–16032. [[CrossRef](#)] [[PubMed](#)]
18. Wen, X.; Shi, L.; Wen, G.; Li, Y.; Dong, C.; Yang, J.; Shuang, S. Green synthesis of carbon nanodots from cotton for multicolor imaging, patterning, and sensing. *Sens. Actuators B* **2015**, *221*, 769–776. [[CrossRef](#)]
19. Zhang, Q.; Xie, S.; Yang, Y.; Wu, Y.; Wang, X.; Wu, J.; Zhang, L.; Chen, J.; Wang, Y. A facile synthesis of highly nitrogen-doped carbon dots for imaging and detection in biological samples. *J. Anal. Methods Chem.* **2018**, *2018*, 1–9. [[CrossRef](#)] [[PubMed](#)]
20. Sachdev, A.; Gopinath, P. Green synthesis of multifunctional carbon dots from coriander leaves and their potential application as antioxidants, sensors and bioimaging agents. *Analyst* **2015**, *140*, 4260–4269. [[CrossRef](#)]
21. Liu, Y.; Liu, Y.; Park, M.; Park, S.; Zhang, Y.; Akanda, M.; Park, B.-Y.; Kim, H. Green synthesis of fluorescent carbon dots from carrot juice for in vitro cellular imaging. *Carbon Lett.* **2017**, *21*, 61–67. [[CrossRef](#)]
22. Zhou, M.; Zhou, Z.; Gong, A.; Zhang, Y.; Li, Q. Synthesis of highly photoluminescent carbon dots via citric acid and Tris for iron(III) ions sensors and bioimaging. *Talanta* **2015**, *143*, 107–113. [[CrossRef](#)]
23. Shen, L.; Zhang, L.; Chen, M.; Chen, X.; Wang, J. The production of pH-sensitive photoluminescent carbon nanoparticles by the carbonization of polyethylenimine and their use for bioimaging. *Carbon* **2013**, *55*, 343–349. [[CrossRef](#)]
24. Chen, B.; Li, F.; Li, S.; Weng, W.; Guo, H.; Guo, T.; Zhang, X.; Chen, Y.; Huang, T.; Hong, X.; et al. Large scale synthesis of photoluminescent carbon nanodots and their application for bioimaging. *Nanoscale* **2013**, *5*, 1967–1971. [[CrossRef](#)]
25. Qu, K.; Wang, J.; Ren, J.; Qu, X. Carbon Dots Prepared by Hydrothermal Treatment of Dopamine as an Effective Fluorescent Sensing Platform for the Label-Free Detection of Iron(III) Ions and Dopamine. *Chem.–Eur. J.* **2013**, *19*, 7243–7249. [[CrossRef](#)]
26. Hsu, P.-; Shih, Z.-; Lee, C.-H.; Chang, H. Synthesis and analytical applications of photoluminescent carbon nanodots. *Green Chem.* **2012**, *14*, 917–920. [[CrossRef](#)]

27. Liu, C.; Zhang, P.; Tian, F.; Li, W.; Li, F.; Liu, W. One-step synthesis of surface passivated carbon nanodots by microwave assisted pyrolysis for enhanced multicolor photoluminescence and bioimaging. *J. Mater. Chem.* **2011**, *21*, 13163–13167. [[CrossRef](#)]
28. Xinyue, Z.; Mingyue, J.; Na, N.; Zhijun, C.; Shujun, L.; Shouxin, L.; Jian, L. Natural-product-derived carbon dots: From natural products to functional materials. *ChemSusChem* **2018**, *11*, 11–24. [[CrossRef](#)]
29. Zheng, X.; Ananthanarayanan, A.; Luo, K.; Chen, P. Glowing graphene quantum dots and carbon dots: Properties, syntheses, and biological applications. *Small* **2015**, *11*, 1620–1636. [[CrossRef](#)]
30. Das, P.; Bose, M.; Ganguly, S.; Mondal, S.; Das, A.; Banerjee, S.; Das, N. Green approach to photoluminescent carbon dots for imaging of gram-negative bacteria *Escherichia coli*. *Nanotechnology* **2017**, *28*, 195501. [[CrossRef](#)]
31. Pal, T.; Mohiyuddin, S.; Packirisamy, G. Facile and green synthesis of multicolor fluorescence carbon dots from curcumin: In vitro and in vivo bioimaging and other applications. *ACS Omega* **2018**, *3*, 831–843. [[CrossRef](#)] [[PubMed](#)]
32. Baig, M.; Chen, Y. Bright carbon dots as fluorescence sensing agents for bacteria and curcumin. *J. Colloid Interface Sci.* **2017**, *501*, 341–349. [[CrossRef](#)]
33. Pathak, A.; Pv, S.; Stanley, J.; Satheesh Babu, T. Multicolor emitting N/S-doped carbon dots as a fluorescent probe for imaging pathogenic bacteria and human buccal epithelial cells. *Microchim. Acta* **2019**, *186*, 157. [[CrossRef](#)] [[PubMed](#)]
34. Wang, J.; Liu, X.; Milcovich, G.; Chen, T.; Durack, E.; Mallen, S.; Yongming, R.; Weng, X.; Hudson, S. Co-reductive fabrication of carbon nanodots with high quantum yield for bioimaging of bacteria. *Beilstein J. Nanotechnol.* **2018**, *9*, 137–145. [[CrossRef](#)] [[PubMed](#)]
35. Yang, J.; Zhang, X.; Ma, Y.; Gao, G.; Chen, X.; Jia, H.-R.; Li, Y.; Chen, Z.; Wu, F. Carbon dot-based platform for simultaneous bacterial distinguishment and antibacterial applications. *ACS Appl. Mater. Interfaces* **2016**, *8*, 32170–32181. [[CrossRef](#)]
36. Nandi, S.; Ritenberg, M.; Jelinek, R. Bacterial detection with amphiphilic carbon dots. *Analyst* **2015**, *140*, 4232–4237. [[CrossRef](#)] [[PubMed](#)]
37. Lu, F.; Song, Y.; Huang, H.; Liu, Y.; Fu, Y.; Huang, J.; Li, H.; Qu, H.; Kang, Z. Fluorescent carbon dots with tunable negative charges for bio-imaging in bacterial viability assessment. *Carbon* **2017**, *120*, 95–102. [[CrossRef](#)]
38. Song, Y.; Li, H.; Lu, F.; Wang, H.; Zhang, M.; Yang, J.; Huang, J.; Huang, H.; Liu, Y.; Kang, Z. Fluorescent carbon dots with highly negative charges as a sensitive probe for real-time monitoring of bacterial viability. *J. Mater. Chem. B* **2017**, *5*, 6008–6015. [[CrossRef](#)]
39. Hua, X.; Bao, Y.; Wang, H.; Chen, Z.; Wu, F. Bacteria-derived fluorescent carbon dots for microbial live/dead differentiation. *Nanoscale* **2017**, *9*, 2150–2161. [[CrossRef](#)]
40. Bhamore, J.; Jha, S.; Park, T.; Kailasa, S. Green synthesis of multi-color emissive carbon dots from Manilkara zapota fruits for bioimaging of bacterial and fungal cells. *J. Photochem. Photobiol. B* **2019**, *191*, 150–155. [[CrossRef](#)]
41. Kasibabu, B.; D'Souza, S.; Jha, S.; Singhal, R.; Basu, H.; Kailasa, S. One-step synthesis of fluorescent carbon dots for imaging bacterial and fungal cells. *Anal. Methods* **2015**, *7*, 2373–2378. [[CrossRef](#)]
42. Kasibabu, B.; D'souza, S.; Jha, S.; Kailasa, S. Imaging of bacterial and fungal cells using fluorescent carbon dots prepared from *Carica papaya* juice. *J. Fluoresc.* **2015**, *25*, 803–810. [[CrossRef](#)]
43. Hola, K.; Zhang, Y.; Wang, Y.; Giannelis, E.; Zboril, R.; Rogach, A. Carbon dots—Emerging light emitters for bioimaging, cancer therapy and optoelectronics. *Nano Today* **2014**, *9*, 590–603. [[CrossRef](#)]
44. Du, F.; Li, J.; Hua, Y.; Zhang, M.; Zhou, Z.; Yuan, J.; Wang, J.; Peng, W.; Zhang, L.; Xia, S.; et al. Multicolor Nitrogen-Doped Carbon Dots for Live Cell Imaging. *J. Biomed. Nanotechnol.* **2015**, *11*, 780–788. [[CrossRef](#)]
45. Karakoçak, B.; Liang, J.; Kavadiya, S.; Berezin, M.; Biswas, P.; Ravi, N. Optimizing the synthesis of red-emissive nitrogen-doped carbon dots for use in bioimaging. *ACS Appl. Nano Mater.* **2018**, *1*, 3682–3692. [[CrossRef](#)]
46. Xu, X.; Zhang, K.; Zhao, L.; Li, C.; Bu, W.; Shen, Y.; Gu, Z.; Chang, B.; Zheng, C.; Lin, C.; et al. Aspirin-based carbon dots, a good biocompatibility of material applied for bioimaging and anti-inflammation. *ACS Appl. Mater. Interfaces* **2016**, *8*, 32706–32716. [[CrossRef](#)]
47. Yao, H.; Li, J.; Song, Y.; Zhao, H.; Wei, Z.; Li, X.; Jin, Y.; Yang, B.; Jiang, J. Synthesis of ginsenoside Re-based carbon dots applied for bioimaging and effective inhibition of cancer cells. *Int. J. Nanomed.* **2018**, *13*, 6249–6264. [[CrossRef](#)]

48. Niu, N.; Ma, Z.; He, F.; Li, S.; Li, J.; Liu, S.; Yang, P. Preparation of carbon dots for cellular imaging by the molecular aggregation of cellulolytic enzyme lignin. *Langmuir* **2017**, *33*, 5786–5795. [[CrossRef](#)]
49. Tripathi, K.; Tran, T.; Tung, T.; Losic, D.; Kim, T. Water soluble Fluorescent Carbon Nano Dots from Bio-Source for Cells Imaging. *J. Nanomater.* **2016**, 2017. [[CrossRef](#)]
50. He, G.; Xu, M.; Mengjun, S.; Li, X.; Yang, Z.; Zhang, L.; Su, Y.; Hu, N.; Zhang, Y. Rapid solid-phase microwave synthesis of highly photoluminescent nitrogen-doped carbon dots for Fe⁽³⁺⁾ detection and cellular bioimaging. *Nanotechnology* **2016**, *27*, 395706. [[CrossRef](#)]
51. Emam, A.; Loutfy, S.; Mostafa, A.; Awad, H.; Mohamed, M. Cyto-toxicity, biocompatibility and cellular response of carbon dots–plasmonic based nano-hybrids for bioimaging. *RSC Adv.* **2017**, *7*, 23502–23514. [[CrossRef](#)]
52. Li, L.; Lu, C.; Li, S.; Liu, S.; Wang, L.; Cai, W.; Xu, W.; Yang, X.; Liu, Y.; Zhang, R. A high-yield and versatile method for the synthesis of carbon dots for bioimaging applications. *J. Mater. Chem. B* **2017**, *5*, 1935–1942. [[CrossRef](#)]
53. Yang, W.; Zhang, H.; Lai, J.; Peng, X.; Hu, Y.; Gu, W.; Ye, L. Carbon dots with red-shifted photoluminescence by fluorine doping for optical bio-imaging. *Carbon* **2018**, *128*, 78–85. [[CrossRef](#)]
54. Xue, B.; Yang, Y.; Sun, Y.; Fan, J.; Li, X.; Zhang, Z. Photoluminescent lignin hybridized carbon quantum dots composites for bioimaging applications. *Int. J. Biol. Macromol.* **2019**, *122*, 954–961. [[CrossRef](#)] [[PubMed](#)]
55. Niu, W.; Li, Y.; Zhu, R.; Shan, D.; Fan, Y.; Zhang, X. Ethylenediamine-assisted hydrothermal synthesis of nitrogen-doped carbon quantum dots as fluorescent probes for sensitive biosensing and bioimaging. *Sens. Actuators B* **2015**, *218*, 229–236. [[CrossRef](#)]
56. Zou, W.; Ji, Y.; Wang, X.; Zhao, Q.; Zhang, J.; Shao, Q.; Liu, J.; Wang, F.; Wang, Y. Insecticide as a precursor to prepare highly bright carbon dots for patterns printing and bioimaging: A new pathway for making poison profitable. *Chem. Eng. J.* **2016**, *294*, 323–332. [[CrossRef](#)]
57. Atchudan, R.; Jebakumar Immanuel Edison, T.N.; Rok Lee, Y. Nitrogen-doped carbon dots originating from unripe peach for fluorescent bioimaging and electrocatalytic oxygen reduction reaction. *J. Colloid. Interface Sci.* **2016**, *482*, 8–18. [[CrossRef](#)] [[PubMed](#)]
58. Sadhanala, H.; Nanda, K. Boron-doped carbon nanoparticles: Size-independent color tunability from red to blue and bioimaging applications. *Carbon* **2016**, *96*, 166–173. [[CrossRef](#)]
59. Puvvada, N.; Kumar, B.; Konar, S.; Kalita, H.; Mandal, M.; Mahanty, A.P. Synthesis of biocompatible multicolor luminescent carbon dots for bioimaging applications. *Sci. Technol. Adv. Mater.* **2012**, *13*, 045008. [[CrossRef](#)]
60. Yang, C.; Thomsen, R.; Ogaki, R.; Kjems, J.; Teo, B. Ultrastable green fluorescence carbon dots with a high quantum yield for bioimaging and use as theranostic carriers. *J. Mater. Chem. B* **2015**, *3*, 4577–4584. [[CrossRef](#)]
61. Zhang, M.; Chi, C.; Yuan, P.; Su, Y.; Shao, M.; Zhou, N. A hydrothermal route to multicolor luminescent carbon dots from adenosine disodium triphosphate for bioimaging. *Mater. Sci. Eng. C* **2017**, *76*, 1146–1153. [[CrossRef](#)] [[PubMed](#)]
62. Yu, T.; Wang, H.; Guo, C.; Zhai, Y.; Yang, J.; Yuan, J. A rapid microwave synthesis of green-emissive carbon dots with solid-state fluorescence and pH-sensitive properties. *R. Soc. Open Sci.* **2018**, *5*, 180245. [[CrossRef](#)]
63. Wang, C.; Xu, Z.; Zhang, C. Polyethyleneimine-functionalized fluorescent carbon dots: Water stability, pH sensing, and cellular imaging. *ChemNanoMat* **2015**, *1*, 122–127. [[CrossRef](#)]
64. Chandra, S.; Das, P.; Bag, S.; Laha, D.; Pramanik, P. Synthesis, functionalization and bioimaging applications of highly fluorescent carbon nanoparticles. *Nanoscale* **2011**, *3*, 1533–1540. [[CrossRef](#)]
65. Wang, F.; Xie, Z.; Zhang, H.; Liu, C.; Zhang, Y. Highly Luminescent Organosilane-Functionalized Carbon Dots. *Adv. Funct. Mater.* **2011**, *21*, 1027–1031. [[CrossRef](#)]
66. Loukanov, A.; Mladenova, P.; Toshev, S.; Karailiev, A.; Ustinovich, E.; Nakabayashi, S. Real time monitoring and quantification of uptake carbon nanodots in eukaryotic cells. *Microsc. Res. Tech.* **2018**, *81*, 1541–1547. [[CrossRef](#)]
67. Shakhov, A.; Astafiev, A.; Osychenko, A.; Syrchina, M.; Nadtochenko, V. Live cell bioimaging with carbon dots produced in situ by femtosecond laser from intracellular material. *bioRxiv* **2019**. [[CrossRef](#)]
68. Jung, Y.; Shin, E.; Kim, B. Cell nucleus-targeting zwitterionic carbon dots. *Sci. Rep.* **2015**, *5*, 18807. [[CrossRef](#)]
69. Yang, L.; Jiang, W.; Qiu, L.; Jiang, X.; Zuo, D.; Wang, D.; Yang, L. One pot synthesis of highly luminescent polyethylene glycol anchored carbon dots functionalized with a nuclear localization signal peptide for cell nucleus imaging. *Nanoscale* **2015**, *7*, 6104–6113. [[CrossRef](#)]

70. Hua, X.; Bao, Y.; Wu, F. Fluorescent carbon quantum dots with intrinsic nucleolus-targeting capability for nucleolus imaging and enhanced cytosolic and nuclear drug delivery. *ACS Appl. Mater. Interfaces* **2018**, *10*, 10664–10677. [[CrossRef](#)]
71. He, H.; Wang, Z.; Cheng, T.; Liu, X.; Wang, X.; Wang, J.; Ren, H.; Sun, Y.; Song, Y.; Yang, J.; et al. Visible and near-infrared dual-emission carbogenic small molecular complex with high rna selectivity and renal clearance for nucleolus and tumor imaging. *ACS Appl. Mater. Interfaces* **2016**, *8*, 28529–28537. [[CrossRef](#)]
72. Chen, M.; Wang, W.; Wu, X. One-pot green synthesis of water-soluble carbon nanodots with multicolor photoluminescence from polyethylene glycol. *J. Mater. Chem. B* **2014**, *2*, 3937–3945. [[CrossRef](#)]
73. Yuan, M.; Guo, Y.; Wei, J.; Li, J.; Long, T.; Liu, Z. Optically active blue-emitting carbon dots to specifically target the Golgi apparatus. *RSC Adv.* **2017**, *7*, 49931–49936. [[CrossRef](#)]
74. Wang, B.; Wang, Y.; Wu, H.; Song, X.; Guo, X.; Zhang, D.; Ma, X.; Tan, M. A mitochondria-targeted fluorescent probe based on TPP-conjugated carbon dots for both one- and two-photon fluorescence cell imaging. *RSC Adv.* **2014**, *4*, 49960–49963. [[CrossRef](#)]
75. Zhang, Y.; Shen, Y.; Teng, X.; Yan, M.; Bi, H.; Morais, P.C. Mitochondria-targeting nanoplatform with fluorescent carbon dots for long time imaging and magnetic field-enhanced cellular uptake. *ACS Appl. Mater. Interfaces* **2015**, *7*, 10201–10212. [[CrossRef](#)]
76. Du, F.; Min, Y.; Zeng, F.; Yu, C.; Wu, S. A Targeted and FRET-based ratiometric fluorescent nanoprobe for imaging mitochondrial hydrogen peroxide in living cells. *Small* **2014**, *10*, 964–972. [[CrossRef](#)]
77. Xu, J.; Zeng, F.; Wu, H.; Hu, C.; Yu, C.; Wu, S. Preparation of a mitochondria-targeted and no-releasing nanoplatform and its enhanced pro-apoptotic effect on cancer cells. *Small* **2014**, *10*, 3750–3760. [[CrossRef](#)]
78. Jiang, X.; Zong, S.; Chen, C.; Zhang, Y.; Wang, Z.; Cui, Y. Gold-carbon dots for the intracellular imaging of cancer-derived exosomes. *Nanotechnology* **2018**, *29*, 175701. [[CrossRef](#)] [[PubMed](#)]
79. Lu, W.; Gong, X.; Nan, M.; Liu, Y.; Shuang, S.; Dong, C. Comparative study for N and S doped carbon dots: Synthesis, characterization and applications for Fe³⁺ probe and cellular imaging. *Anal. Chim. Acta* **2015**, *898*, 116–127. [[CrossRef](#)] [[PubMed](#)]
80. Chen, Y.; Wu, Y.; Weng, B.; Wang, B.; Li, C. Facile synthesis of nitrogen and sulfur codoped carbon dots and application for Fe(III) ions detection and cell imaging. *Sens. Actuators B* **2016**, *223*, 689–696. [[CrossRef](#)]
81. Kaur, H.; Raj, P.; Sharma, H.; Verma, M.; Singh, N.; Kaur, N. Highly selective and sensitive fluorescence sensing of nanomolar Zn²⁺ ions in aqueous medium using Calix[4]arene passivated carbon quantum dots based on fluorescence enhancement: Real-time monitoring and intracellular investigation. *Anal. Chim. Acta* **2018**, *1009*, 1–11. [[CrossRef](#)] [[PubMed](#)]
82. Kong, D.; Yan, F.; Luo, Y.; Ye, Q.; Zhou, S.; Chen, L. Amphiphilic carbon dots for sensitive detection, intracellular imaging of Al³⁺. *Anal. Chim. Acta* **2017**, *953*, 63–70. [[CrossRef](#)]
83. Zhang, L.; Wang, Z.; Zhang, J.; Jia, J.; Zhao, D.; Fan, Y. Phenanthroline-derivative functionalized carbon dots for highly selective and sensitive detection of Cu²⁺ and S²⁻ and imaging inside live cells. *Nanomaterials* **2018**, *8*, 1071. [[CrossRef](#)] [[PubMed](#)]
84. Kiran, S.; Misra, R. Mechanism of intracellular detection of glucose through nonenzymatic and boronic acid functionalized carbon dots. *J. Biomed. Mater. Res. A* **2015**, *103*, 2888–2897. [[CrossRef](#)] [[PubMed](#)]
85. Liu, Y.; Tian, Y.; Tian, Y.; Wang, Y.; Yang, W. Carbon-dot-based nanosensors for the detection of intracellular redox state. *Adv. Mater.* **2015**, *27*, 7156–7160. [[CrossRef](#)]
86. Shi, W.; Guo, F.; Han, M.; Yuan, S.; Guan, W.; Li, H.; Huang, H.; Liu, Y.; Kang, Z. N,S codoped carbon dots as a stable bio-imaging probe for detection of intracellular temperature and tetracycline. *J. Mater. Chem. B* **2017**, *5*, 3293–3299. [[CrossRef](#)]
87. Kalytchuk, S.; Poláková, K.; Wang, Y.; Froning, J.; Cepe, K.; Rogach, A.; Zbořil, R. Carbon dot nanothermometry: Intracellular photoluminescence lifetime thermal sensing. *ACS Nano* **2017**, *11*, 1432–1442. [[CrossRef](#)]
88. Shangguan, J.; He, D.; He, X.; Wang, K.; Xu, F.; Liu, J.; Tang, J.; Yang, X.; Huang, J. Label-free carbon-dots-based ratiometric fluorescence ph nanoprobes for intracellular pH sensing. *Anal. Chem.* **2016**, *88*, 7837–7843. [[CrossRef](#)] [[PubMed](#)]
89. Chandra, A.; Singh, N. Biocompatible fluorescent carbon dots for ratiometric intracellular ph sensing. *ChemistrySelect* **2017**, *2*, 5723–5728. [[CrossRef](#)]

90. Zholobak, N.; Popov, A.; Shcherbakov, A.; Popova, N.; Guzyk, M.; Antonovich, V.; Yegorova, A.; Scrypynets, Y.; Leonenko, I.; Baranchikov, A.; et al. Facile fabrication of luminescent organic dots by thermolysis of citric acid in urea melt, and their use for cell staining and polyelectrolyte microcapsule labelling. *Beilstein J. Nanotechnol.* **2016**, *7*, 1905–1917. [[CrossRef](#)]
91. Liu, H.; Li, Z.; Sun, Y.; Geng, X.; Hu, Y.; Meng, H.; Ge, J.; Qu, L. Synthesis of luminescent carbon dots with ultrahigh quantum yield and inherent folate receptor-positive cancer cell targetability. *Sci. Rep.* **2018**, *8*, 1086. [[CrossRef](#)] [[PubMed](#)]
92. Bhunia, S.; Maity, A.; Nandi, S.; Stepensky, D.; Jelinek, R. Imaging cancer cells expressing the folate receptor with carbon dots produced from folic acid. *ChemBioChem* **2016**, *17*, 614–619. [[CrossRef](#)]
93. Wang, Z.; Fu, B.; Zou, S.; Duan, B.; Chang, C.; Yang, B.; Zhou, X.; Zhang, L. Facile construction of carbon dots via acid catalytic hydrothermal method and their application for target imaging of cancer cells. *Nano Res.* **2016**, *9*, 214–223. [[CrossRef](#)]
94. Motaghi, H.; Mehrgardi, M.; Bouvet, P. Carbon dots-AS1411 aptamer nanoconjugate for ultrasensitive spectrofluorometric detection of cancer cells. *Sci. Rep.* **2017**, *7*, 10513. [[CrossRef](#)] [[PubMed](#)]
95. Kang, Z.; Liu, Y.; Lee, S. Carbon dots for bioimaging and biosensing applications. In *Carbon-Based Nanosensor Technology*; Kranz, C., Ed.; Springer: Cham, Switzerland, 2017; Volume 17. [[CrossRef](#)]
96. Yang, S.; Cao, L.; Luo, P.; Lu, F.; Wang, X.; Wang, H.; Mezziani, M.; Liu, Y.; Qi, G.; Sun, Y. Carbon dots for optical imaging in vivo. *J. Am. Chem. Soc.* **2009**, *131*, 11308–11309. [[CrossRef](#)]
97. Kuo, T.; Sung, S.; Hsu, C.; Chang, C.; Chiu, T.; Hu, C. One-pot green hydrothermal synthesis of fluorescent nitrogen-doped carbon nanodots for in vivo bioimaging. *Anal. Bioanal. Chem.* **2016**, *408*, 77–82. [[CrossRef](#)] [[PubMed](#)]
98. Zheng, M.; Ruan, S.; Liu, S.; Sun, T.; Qu, D.; Zhao, H.; Xie, Z.; Gao, H.; Jing, X.; Sun, Z. Self-targeting fluorescent carbon dots for diagnosis of brain cancer cells. *ACS Nano* **2015**, *9*, 11455–11461. [[CrossRef](#)] [[PubMed](#)]
99. Ren, W.; Chen, S.; Liao, Y.; Li, S.; Ge, J.; Tao, F.; Huo, Q.; Zhang, Y.; Zhao, Z. Near-infrared fluorescent carbon dots encapsulated liposomes as multifunctional nano-carrier and tracer of the anticancer agent cinobufagin in vivo and in vitro. *Colloids Surf. B* **2019**, *174*, 384–392. [[CrossRef](#)]
100. Lan, M.; Zhao, S.; Zhang, Z.; Yan, L.; Guo, L.; Niu, G.; Zhang, J.; Zhao, J.; Zhang, H.; Wang, P.; et al. Two-photon-excited near-infrared emissive carbon dots as multifunctional agents for fluorescence imaging and photothermal therapy. *Nano Res.* **2017**, *10*, 3113–3123. [[CrossRef](#)]
101. Zhang, W.; Wang, R.; Liu, W.; Wang, X.; Li, P.; Zhang, W.; Wang, H.; Tang, B. Te-containing carbon dots for fluorescence imaging of superoxide anion in mice during acute strenuous exercise or emotional changes. *Chem. Sci.* **2018**, *9*, 721–727. [[CrossRef](#)]
102. Wei, X.; Xu, Y.; Li, Y.; Yin, X.; He, X. Ultrafast synthesis of nitrogen-doped carbon dots via neutralization heat for bioimaging and sensing applications. *RSC Adv.* **2014**, *4*, 44504–44508. [[CrossRef](#)]
103. Kang, Y.; Li, Y.; Fang, Y.; Xu, Y.; Wei, X.; Yin, X. Carbon quantum dots for zebrafish fluorescence imaging. *Sci. Rep.* **2015**, *5*, 11835. [[CrossRef](#)] [[PubMed](#)]
104. Li, S.; Peng, Z.; Dallman, J.; Baker, J.; Othman, A.; Blackwelder, P.; Leblanc, R. Crossing the blood–brain–barrier with transferrin conjugated carbon dots: A zebrafish model study. *Colloids Surf. B* **2016**, *145*, 251–256. [[CrossRef](#)]
105. Wei, X.; Li, L.; Liu, J.; Yu, L.; Li, H.; Cheng, F.; Yi, X.; He, J.; Li, B. Green Synthesis of Fluorescent Carbon Dots from Gynostemma for Bioimaging and Antioxidant in Zebrafish. *ACS Appl. Mater. Interfaces* **2019**, *11*, 9832–9840. [[CrossRef](#)] [[PubMed](#)]
106. Li, S.; Skromne, I.; Peng, Z.; Dallman, J.; Al-Youbi, A.; Bashammakh, A.; El-Shahawi, M.; Leblanc, R. “Dark” carbon dots specifically “light-up” calcified zebrafish bones. *J. Mater. Chem. B* **2016**, *4*, 7398–7405. [[CrossRef](#)]
107. Saxena, M.; Sonkar, S.; Sarkar, S. Water soluble nanocarbons arrest the growth of mosquitoes. *RSC Adv.* **2013**, *3*, 22504–22508. [[CrossRef](#)]

